

2D site response simulation of Heathcote Valley during the 2010-2011 Canterbury earthquake sequence

S. Jeong¹, B.A. Bradley²

ABSTRACT

The strong motion station at Heathcote Valley School (HVSC) recorded unusually high peak ground accelerations (2.21g vertical and 1.41g horizontal) during the February 2011 Christchurch earthquake. Ground motions recorded at HVSC in numerous other events also exhibited consistently higher intensities compared with nearby strong motion stations. The characteristics of the valley dynamic response at HVSC were investigated by means of 2D dynamic finite element analyses, where recorded motions at LPCC (Lyttelton Port Company station) are used as input motions for the analyses. The simulations agree well with observed motions and suggest that the motions at HVSC are amplified in a wide band of frequencies. Simulations suggest that strong non-linear response of soils reduced the amplification at $f = 4$ -10 Hz, likely due to the increased energy dissipation. Sensitivity analyses demonstrate the importance of accurate site characterization for a successful prediction of the site response.

Introduction

Numerous intense ground motions were recorded during the 22 February 2011 Christchurch earthquake. Peak ground acceleration recorded at Heathcote Valley School station (HVSC) exceeded 2g in vertical component, and 1.4g in horizontal component (Bradley & Cubrinovski 2011). Other ground motions recorded at HVSC during the 2010-2011 Canterbury earthquake sequence also exhibited consistently higher intensities compared with nearby strong motion stations (Bradley 2012; Bradley 2013).

Figure 1 provides a comparison of ground motions recorded at Heathcote Valley School station and the nearby Lyttelton Port Company station (LPCC) in the three largest shaking events in the earthquake sequence. The locations of these two stations are shown in Figure 2.

HVSC is located close to the edge of Heathcote Valley, where shallow, firm colluvium sediments mantle weathered volcanic rock. Heathcote Valley is a V-shaped valley facing north, surrounded by the volcanic Port Hills. Fine silts (loess)—originating from glacial and river erosion of the Southern Alps during the cold cycles of the Quaternary—are predominant in surficial soils in the Port Hills area, which were deposited by Aeolian process and then washed down to the valley along with volcanic rock debris to form the colluvium (Brown *et al.* 1992). The thickness of surficial soil varies from a few meters on the ridges to 20-30 meters in the valleys.

In this paper, a case study of site amplification effects at Heathcote Valley from observations

¹Postdoctoral Fellow, Department of Civil and Natural Resources Engineering, University of Canterbury, Christchurch, New Zealand, seokho.jeong@canterbury.ac.nz

²Associate Professor, Department of Civil and Natural Resources Engineering, University of Canterbury, Christchurch, New Zealand, brendon.bradley@canterbury.ac.nz

and numerical simulations is presented. A brief summary of the geophysical and geotechnical site characterization is first presented, followed by presentation of the salient results from a series of 2D site response analyses to investigate the effects of the soil non-linearity, the valley stratigraphy, surface topography, and the soil-bedrock impedance contrast on the simulated intensity of ground shaking at HVSC as compared to observations.

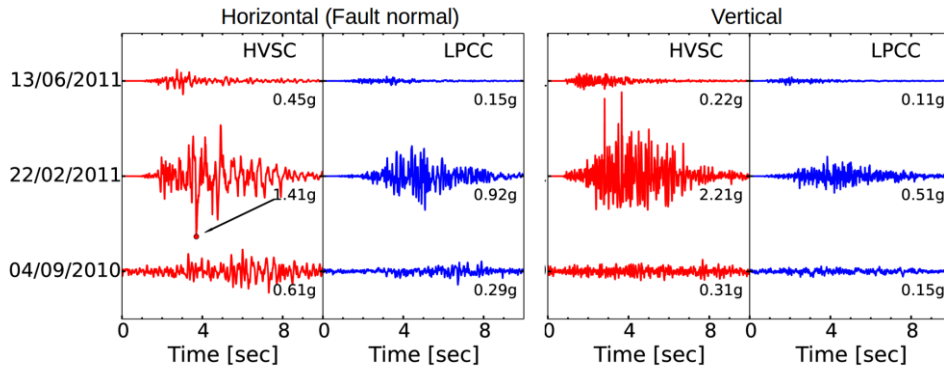


Figure 1. Comparison of horizontal (fault normal component) and vertical acceleration time histories recorded at HVSC and LPCC over the three largest shaking events in the Canterbury earthquake sequence (all acceleration amplitudes to scale with maximum values shown).

Site Characterization

Fifteen seismic cone penetration tests (sCPT) and five multichannel analyses of surface waves (MASW) surveys were performed at Heathcote Valley, the locations of which are plotted in Figure 2. A LiDAR-based digital elevation model was used to account for the surface topography. The sCPT results, summarized in Figure 3a, suggest that shear wave velocity, V_S , is strongly depth dependent, a typical characteristic of non-plastic granular materials. This depth dependence is modelled by a power law equation as shown in Figure 3a where z is depth below ground surface:

$$V_S = 144 z^{0.39} \quad (1)$$

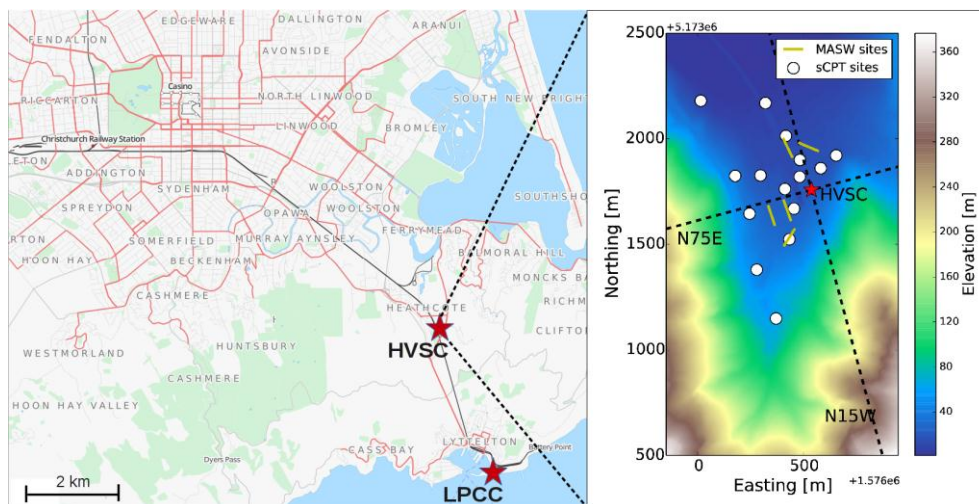


Figure 2. Location and topography of Heathcote valley, strong motion stations, and test sites.

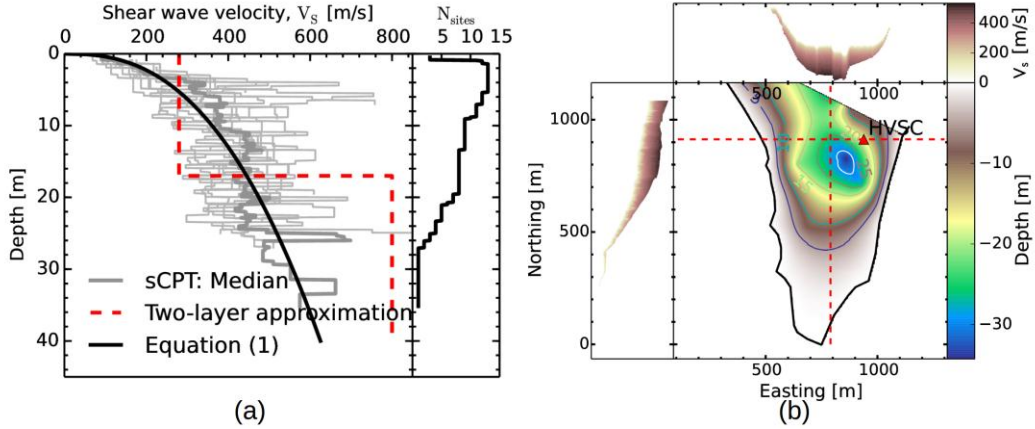


Figure 3. (a) Shear wave velocity of the loess colluvium at 15 locations in Heathcote Valley as function of depth. At every depth interval, N_{sites} indicates the number of sites with available data; (b) a contour plot of sediment depth obtained by interpolation of sCPT and MASW data. Subaxes on top and on the left of the main plot show valley cross sections along the red dashed lines, with contours of V_S approximated by Equation 1.

A simplified two layer version of the velocity profile at HVSC is also shown in Figure 3a; the effect of such simplification will be discussed later in this paper. Soil strength parameters ($\phi = 36^\circ$ and $c = 0$ kPa) are estimated from the triaxial test data performed on Port hills loess (Tonkin and Taylor 2012). The thickness of sediments, obtained from CPT refusal depths and corroborated by MASW test results, was spatially interpolated using the ordinary Kriging algorithm (Matheron 1963) to estimate the depth of the weathered volcanic rock over the region of interest, which underlies the surficial sediments. Figure 3b shows a contour plot of sediment depth, in which subaxes on the top and to the left of the main plot show cross sections of the valley with filled contours of V_S , approximated by Equation 1.

Model Description

A series of 2D plane strain finite element analyses were performed using OpenSees (Mazzoni *et al.* 2007) for cross sections of the valley along the two different azimuths shown in Figure 2: N75E (across the valley) and N15W (down the valley). The two valley cross sections showed qualitatively similar responses, and therefore this paper focuses on the simulation of the N75E cross section only. Figure 4 schematically illustrates the mesh geometry and boundary conditions of the numerical model. Lateral boundaries are treated with free-field boundary conditions to minimize spurious reflections. The absorbing boundary at the bottom of the models is achieved via Lysmer dashpots (Kuhlemeyer & Lysmer 1973).

Mass densities are assumed as $\rho_{Soil} = 1.8 \text{ Mg/m}^3$ and $\rho_{Rock} = 2.4 \text{ Mg/m}^3$. Rock layers are modelled with linear-elastic Poisson solids. The inelastic stress-strain behavior of soil is modeled with the pressure dependent multi yield (PDMY) plasticity model (Yang *et al.* 2003). The pressure dependent shear wave velocity of the soil is modelled by Equation 1. The V_S of the weathered rock beneath the soil is estimated from the result of MASW as $V_S = 800$ m/s (although sensitivity studies of the rock profile modelling are presented subsequently). The model assumes the V_S of the halfspace as $V_{SB} = 1520$ m/s, the same as the V_S of the bedrock at LPCC (Wood *et al.* 2011). A stiffness proportional damping is assumed with the critical damping ratio, $\zeta = 0.01$ at the frequency, $f = 16$ Hz.

The model is subjected to nine events recorded during the 2010-2011 Canterbury earthquake sequence which are summarized in Table 1. The acceleration time series recorded at LPCC were deconvolved from one dimensional site response, using the shear wave velocity profile by Wood *et al.* (2011), and used as vertically incident input motions prescribed at the base of model via equivalent nodal forces.

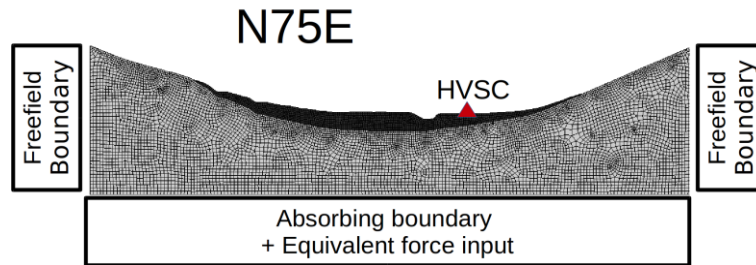


Figure 4. Two-dimensional mesh geometries and boundary conditions of the simulated valley cross section.

Table 1. Earthquake events used in the analyses, in chronological order.

Event date	M_w	HVSC			LPCC		
		R_{rup}^* (km)	PGA** (g)	PGV** (cm/s)	R_{rup}^* (km)	PGA** (g)	PGV** (cm/s)
04/09/2010	7.1	20.8	0.61	29	22.4	0.29	19
19/10/2010	4.8	12.8	0.09	3.2	13.1	0.02	0.71
26/12/2010	4.7	4.7	0.11	2.9	7.7	0.02	0.65
22/02/2011	6.2	3.9	1.41	81	7	0.92	46
16/04/2011	5.0	7.3	0.68	32	5.2	0.29	8.5
13/06/2011 (a)	5.3	4.7	0.45	14	5.3	0.15	5.4
13/06/2011 (b)	6.0	3.6	0.91	55	5.8	0.64	33
21/06/2011	5.2	14.9	0.26	8.0	15.6	0.07	2.1
23/12/2011	5.9	9.7	0.26	42	12.4	0.44	23

*The shortest source-to-site distance based on Beavan *et al.* (2012); **Horizontal components

Comparison with recorded ground motions

Rather than directly comparing the observed and simulated motions at HVSC, we herein compare the median HVSC/LPCC spectral ratios taken over all the considered ground motions. Figure 5 shows the simulated and recorded HVSC/LPCC spectral ratio, expressed principally via the median and \pm std. values over all considered ground motions. Before computing the spectral ratios, the Fourier spectra are smoothed by the Konno & Ohmachi smoothing window (Konno & Ohmachi 1998) with the bandwidth parameter, $b = 40$.

Overall, it can be seen that the comparison is satisfactory, and both the simulation and the observation suggest that ground motions at HVSC are amplified over a broad range of frequencies for both the horizontal and vertical components. However, our numerical simulations under-predicted the horizontal component near $f = 3$ Hz and the vertical

component for $f = 6$ Hz and >10 Hz. The cause of this under-prediction is not yet clear, but it is expected that the limitations of the current model—relatively poor characterization of the dynamic properties of deeper rocks, and the contribution from out-of-plane waves that the model does not account for—would be partially responsible for this discrepancy.

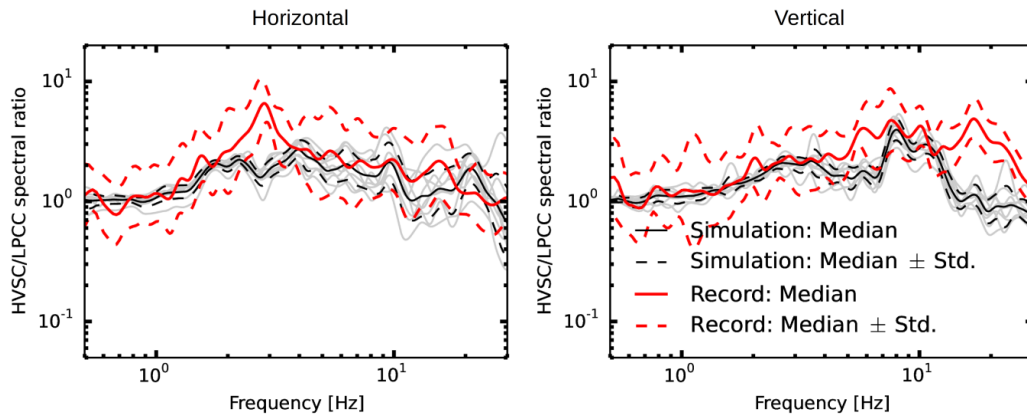


Figure 5. Simulated HVSC/LPCC spectral ratios compared with recorded spectral ratio. Individual simulations are shown in thin grey lines, and the median \pm std. values are given for both the simulations and observations.

Effect of the non-linear soil behavior

Figure 6 shows the comparison of the HVSC/LPCC spectral ratios of simulated results with PDMY soil model and the pressure dependent linear elastic (PDLE) soil model. When all of the nine earthquake events in Table 1 were considered, the effect of soil non-linearity on the median HVSC/LPCC spectral ratio was not significant for frequencies, $f < 10$ Hz. However, the level of maximum inelastic strain of soil (not shown in the paper) was less than 0.05 % for seven out of nine events considered in this study (i.e. non-linear effects were not significant). To better illustrate the effect of soil non-linearity, the median spectral ratio obtained from the three events (22/02/2011, 13/06/2011(b) and 23/12/2011) with maximum ground strain larger than 0.05 % is also plotted in Figure 6 (Sim: PDMY-high intensity), which shows reduction in amplitude in $f = 4$ -10 Hz. A detailed sensitivity study is currently underway to investigate the role of the soil non-linear response on the characteristics of observed ground motions at Heathcote valley.

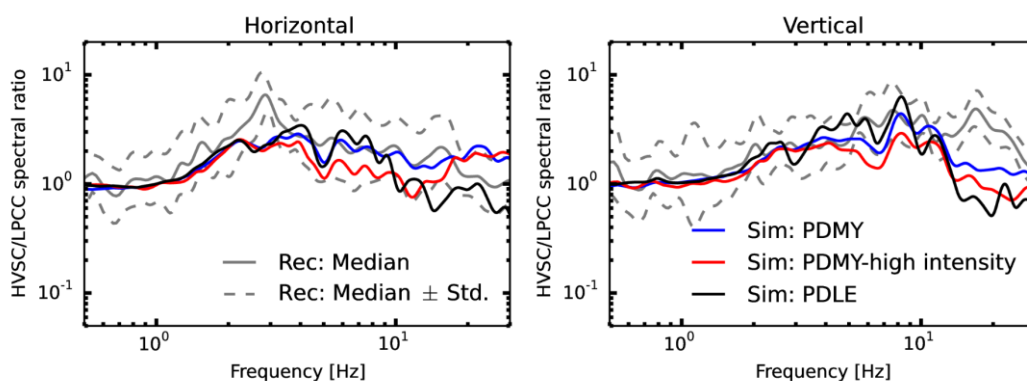


Figure 6. Effect of soil non-linearity on the HVSC/LPCC spectral ratio.

Effect of variations of V_S on the site response at HVSC

A parametric study was conducted to demonstrate the sensitivity of the valley site response to the modelled soil and rock V_S properties. Figure 7 shows the schematic diagram of the valley geometry, and Table 2 lists the velocity profiles considered in the parametric study, which are separately presented in the subsections below.

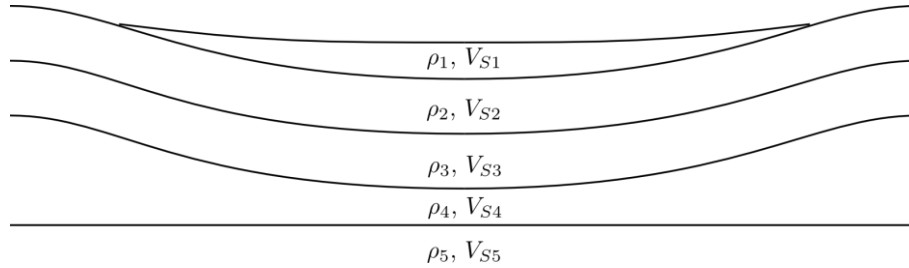


Figure 7. Schematic diagram showing the hypothetical rock velocity profiles.

Table 2. List of velocity profiles considered in this study.

	Profile 1	Profile 2	Profile 3	Profile 4
V_{S1} (m/s)	280	$144 z^{0.39}$	$144 z^{0.39}$	$144 z^{0.39}$
V_{S2} (m/s)	800	800	800	800
V_{S3} (m/s)	800	800	800	1200
V_{S4} (m/s)	800	800	1500	1500
V_{S5} (m/s)	1500	1500	1500	1500

Effect of the pressure dependent shear wave velocity of soils

Figure 8 compares the HVSC/LPCC spectral ratios of Profile 1 with Profile 2, which describes the effect of the pressure dependent shear wave velocity of soils. To solely focus on the effect of pressure dependency, simulations for Figure 8 were performed with linear elastic soil models. The response of the simplified two-layer model was overall comparable with the more realistic power law model (Equation 1). However, results also suggest that the simplified two-layer model overestimates the amplification of vertical motions near $f = 7$ Hz.

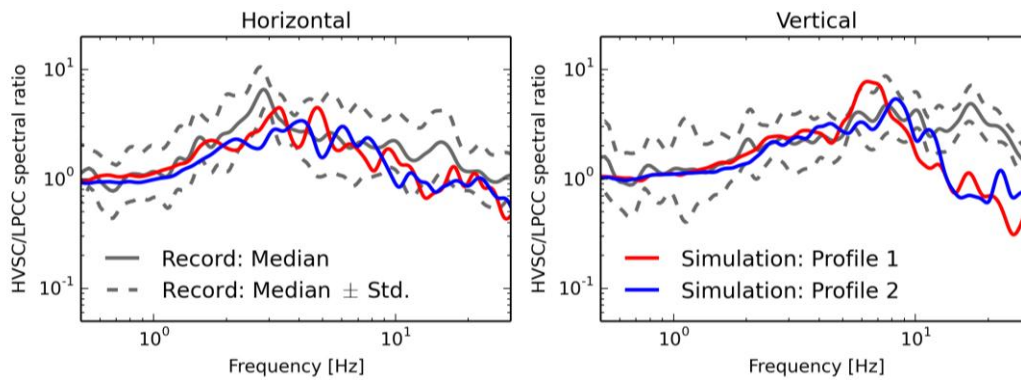


Figure 8. Effect of the pressure dependent shear velocity of the soil.

Effect of rock velocity profiles

The shear wave velocity of the weathered rock was estimated by means of MASW survey. However, our characterization of the rock shear wave velocity is quite poor, due to the practical limitations of MASW survey (i.e. the sledge hammer source has a shallow survey depth, and the passive source MASW requires a wide open space, flat surface topography, and a simple subsurface stratigraphy).

We therefore performed a sensitivity study, using 3 different velocity profiles for the weathered rock layers as described in Table 2 (Profiles 2-4). Figure 9 demonstrates the effect of rock shear wave velocity variations by comparing the HVSC/LPCC spectral ratios of Profile 2, Profile 3, and Profile 4. The result shows that the response at high frequencies (i.e. $f > 3$ Hz for the horizontal component, and $f > 6$ Hz for the vertical component) is not sensitive to the choice of the rock velocity profile. The under-prediction of the valley response shown in Figure 5 more or less remained the same, regardless of the velocity profiles considered in this study. However, the response at lower frequencies was sensitive to the variation of the rock velocity profiles, even though the velocities of the shallowest (V_{S2}) and the deepest (V_{S5}) rock layers are kept constant and the geometry of valley layering is kept simple. The fact that none of the rock profiles realistically model the observed horizontal peak at $f = 3$ Hz indicates that this is likely sensitive to the modelling of the soil layers, which will be further examined in future.

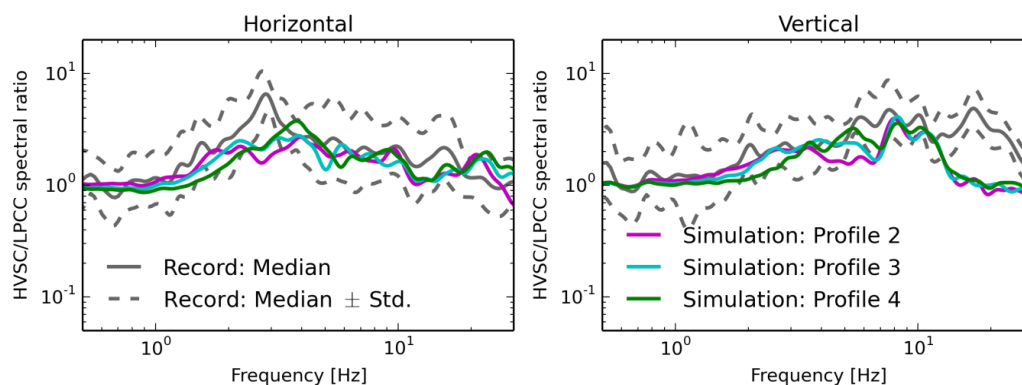


Figure 9. Effect of the rock velocity profile on the median HVSC/LPCC spectral ratios. The uncertainty in the simulated ratios across the considered events is relatively small and omitted for brevity.

Conclusions

This paper presented a case study on the site amplification effects at Heathcote Valley during the 2010-2011 Canterbury earthquake sequence through observations and 2D numerical simulations. A 3D representation of the geological structure of Heathcote Valley was developed using a LiDAR-based DEM and in-situ geophysical test data obtained by sCPT and MASW. Based on the 3D representation of the geological structure, a series of 2D plane strain dynamic finite element simulations were undertaken, assuming that deconvolved motions recorded at LPCC can be used as the input motions at the base of the numerical model.

Both the observation and simulation showed strong amplification over a wide range of

frequencies in both the horizontal and vertical component. Comparisons of simulated and recorded motions demonstrated that the numerical model can simulate the recorded response of the valley at HVSC reasonably well, despite some inherent limitations.

The median spectral ratio from the three events with maximum ground strain larger than 0.05 % showed slightly lower amplitude in $f = 4\text{--}10$ compared with the median of the all considered events, which is likely due to the increased energy dissipation. A more detailed study will be conducted to describe the effect of soil non-linearity on the characteristics of observed ground motions at Heathcote valley.

At Heathcote Valley, the site response at $f < 3$ Hz is largely dominated by the dynamic response of the rock layers, and at $f > 3$ Hz by the soil layers. This study has shown that employing a simplified homogeneous soil model overestimated the vertical response at $f = 7$ Hz, and that the velocities of rock layers need to be accurately characterized if the low frequency ground motions are of importance.

Acknowledgements

Clinton M. Wood (University of Arkansas) kindly provided his MATLAB scripts for the beamforming analyses used in MASW surveys. Matthew Hughes (University of Canterbury) processed the DEM, which was used for modelling the surface topography. Financial support for this research was provided from the New Zealand Earthquake Commission (EQC) and Natural Hazards Research Platform.

References

- Ashford, S.A., Sitar, N., Lysmer, J., & Deng, N. 1997. Topographic effects on the seismic response of steep slopes, *Bull. Seismol. Soc. Am.*, **87**, 701–709.
- Assimaki, D., & Jeong, S. 2013. Ground-Motion Observations at Hotel Montana during the M 7.0 2010 Haiti Earthquake: Topography or Soil Amplification?, *Bull. Seismol. Soc. Am.*, **103**, 2577–2590.
- Beavan, J., Motagh, M., Fielding, E. J., Donnelly, N., & Collett, D. 2012. Fault slip models of the 2010–2011 Canterbury, New Zealand, earthquakes from geodetic data and observations of postseismic ground deformation. *New Zealand Journal of Geology and Geophysics*, **55**(3), 207–221.
- Bradley, B.A. 2012. Strong ground motion characteristics observed in the 4 September 2010 Darfield, New Zealand earthquake. *Soil Dynamics and Earthquake Engineering*, **42**, 32–46.
- Bradley, B.A. 2013. Systematic ground motion observations in the Canterbury earthquakes and region-specific non-ergodic empirical ground motion modeling, *Earthq. Spectra*, 131230112032001, doi:10.1193/053013EQS137M.
- Bradley, B.A., & Cubrinovski, M. 2011. Near-source Strong Ground Motions Observed in the 22 February 2011 Christchurch Earthquake, *Seismol. Res. Lett.*, **82**, 853–865, doi:10.1785/gssrl.82.6.853.
- Brown, L.J., Reay, M.B. & Weeber, J.H. 1992. *Geology of the Christchurch urban area*, Institute of Geological and Nuclear Sciences.
- Johnson, D.H., & Dudgeon, D.E. 1992. *Array signal processing: concepts and techniques*, Simon & Schuster.
- Kawase, H. 1996. The cause of the damage belt in Kobe: “The basin-edge effect,” constructive interference of the direct S-wave with the basin-induced diffracted/Rayleigh waves, *Seismol. Res. Lett.*, **67**(5), 25–34.
- Konno, K., & Ohmachi, T. 1998. Ground-motion characteristics estimated from spectral ratio between horizontal and vertical components of microtremor, *Bull. Seismol. Soc. Am.*, **88**(1), 228–241.
- Kuhlemeyer, R.L., & Lysmer, J. 1973. Finite element method accuracy for wave propagation problems, *J. Soil Mech. & Found. Div.*, 99(Tech Rpt).
- Matheron, G. 1963. Principles of geostatistics, *Econ. Geol.*, **58**(8), 1246–1266.

- Mazzoni, S., McKenna, F., Scott, M.H., & Fenves, G.L. 2007. OpenSees Command Language Manual. Pacific Earthquake Engineering Research Center, *Univ. California, Berkeley*.
- Park, C.B., Miller, R.D., & Xia, J. 1999. Multichannel analysis of surface waves, *Geophysics*, **64**(3), 800–808, doi:10.1190/1.1444590.
- Tonkin and Taylor 2012. Christchurch Earthquake Recovery Geotechnical Factual Report Kinsey / Clifton. Report prepared for the Earthquake Commission. Ref 52010.0400.
- Wathelet, M. 2005. GEOPSY Geophysical Signal Database for Noise Array Processing, *Software, LGIT, Grenoble, Fr.*
- Wood, C.M., Cox, B.R., Wotherspoon, L.M., & Green, R.A. 2011. Dynamic site characterization of Christchurch strong motion stations, *Bull. New Zeal. Soc. Earthq. Eng.*, **44**(4), 195–204.
- Yang, Z., Elgamal, A., & Parra, E. 2003. A computational model for liquefaction and associated shear deformation, *J. Geotechnical and Geoenvironmental Engineering*, **129**(12), 1119-1127.